Quantification of the pelagic primary production beneath Arctic sea ice

Jaclyn Clement Kinney[1*], Wieslaw Maslowski[1], Robert Osinski[2], Meibing Jin[3], Marina Frants[1], Nicole Jeffery[4], Younjoo Lee[1]

[1]Department of Oceanography, Naval Postgraduate School, Monterey, CA, USA; [2]Institute of Oceanology of Polish Academy of Sciences, Sopot, Poland; [3]University of Alaska, Fairbanks, AK, USA; [4]Los Alamos National Laboratories, Los Alamos, NM, USA; *Corresponding author: Jaclyn Clement Kinney (jlclemen@nps.edu)

ABSTRACT

In high-latitude environments such as the Arctic Ocean, phytoplankton growth is strongly constrained by light availability. Because light penetration into the upper ocean is attenuated by snow and ice cover, it was generally believed until recently that phytoplankton growth was limited to areas of open water, with negligible growth under the ice. However, under-ice phytoplankton blooms have been reported multiple times over the past several decades [e.g. Fukuchi et al. (1989); Legendre, Ingram, and Poulin (1989)]. In July 2011, Arrigo et al. (2012) observed a massive phytoplankton bloom beneath sea ice in the Chukchi Sea. Observational evidence suggests that this bloom was not an isolated case, and that under-ice blooms maybe widespread on Arctic continental shelves (Arrigo et al., 2014; Lowry, van Dijken, & Arrigo, 2014). Arrigo and van Dijken (2011) estimate the total primary production north of the Arctic Circle to be 438 +/- 21.5 Tg C yr $^{-1}$. However, due to observational limitations, this estimate did not include under sea ice production. Therefore, an open question remains: How important are under-ice phytoplankton blooms to the total Arctic primary production?

RASM is a high-resolution, fully-coupled, regional model with a domain encompassing the entire marine cryosphere of the Northern Hemisphere, including the major inflow and outflow pathways, with extensions into North Pacific and Atlantic oceans. The components of RASM include: atmosphere, sea ice, ocean, biogeochemical, and land hydrology (Maslowski et al. 2012, Roberts et al. 2015, DuVivier et al. 2016, Hamman et al. 2016, Hamman et al. 2017, Cassano et al. 2017). The ocean BGC component in RASM is a medium-complexity Nutrients-Phytoplankton-Zoo-plankton-Detritus (NPZD) model (Jin et al. 2018). The model has three phytoplankton categories: diatoms, small phytoplankton and diazotrophs.

RASM results show that under-ice pelagic chl-*a* and primary production values can at times be very high, particularly during the spring and early summer. Our numerical model results produce a mean of 495 Tg C yr $^{-1}$ north of the Arctic Circle during 1980-1998 (and 507 Tg C yr $^{-1}$ during 1980-2018). We also see an increase in primary production over the last several decades. This increase is attributed to the reduced sea ice cover, which increases light availability to the upper ocean. We conclude that under-sea-ice pelagic primary production makes up a large fraction of the total production and cannot be considered negligible.

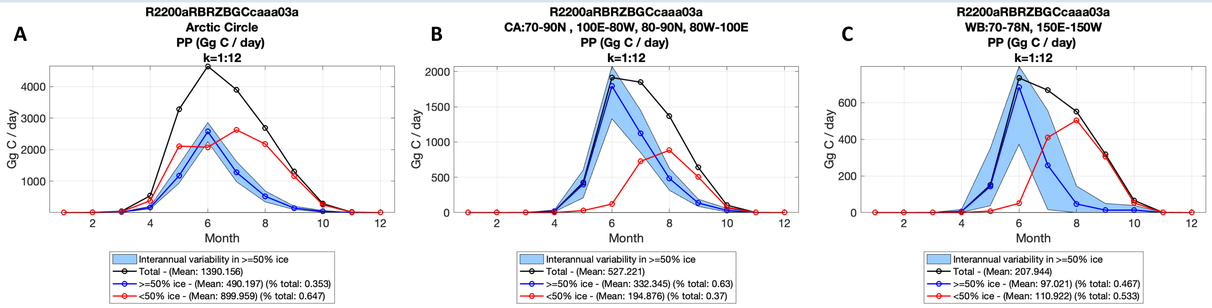

Figure 3. Mean annual cycle of PP (Gg C / d) in the (a) Arctic Circle region, (b) CA region, and (c) WB region over the period 1980-2018. The black line represents the total; the blue line represents production where ice concentration is ≥50%; the red line represents production where ice concentration is <50%. The shaded blue area represents the interannual variability in production where ice concentration is ≥50%.

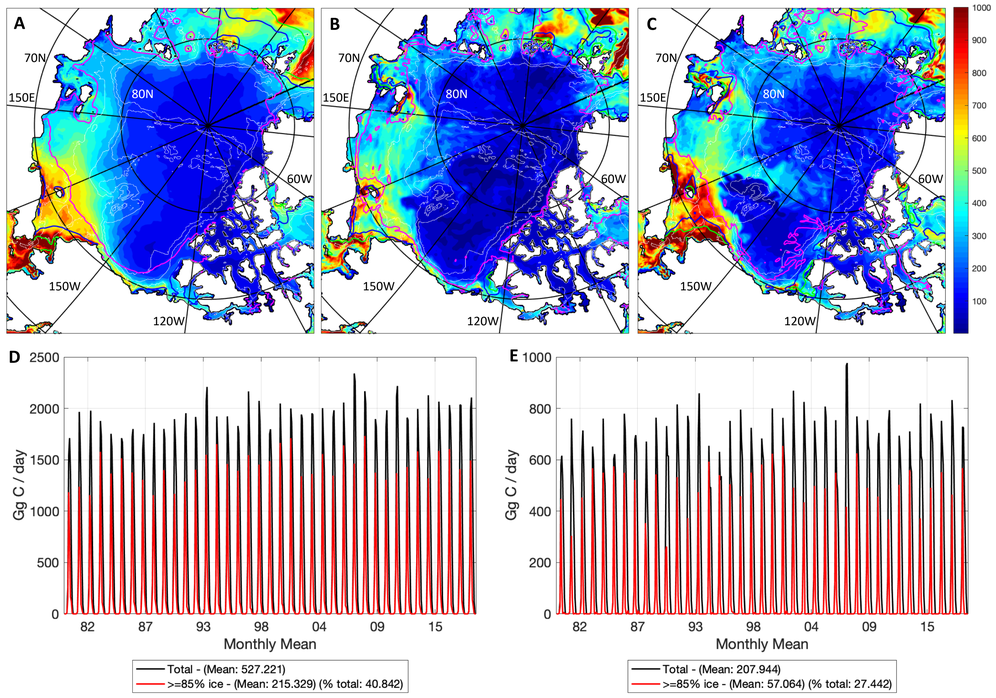

Figure 4. Upper panels: Mean primary production (mg C / m^2 / d) during June averaged over 1980-2018 (a), 1980 (b), and 2011 (c). White contour lines represent bathymetry (50, 500, and 2,000 m); green, blue and magenta contour lines represent ice concentration (15, 50, and 85%, respectively). Lower panels: Time series of monthly mean PP summed over the CA (d) and WB (e) regions (Gg C / d). Red lines represent the sum of PP in grid cells with ice concentration ≥85% and black lines represent the total PP (regardless of ice presence).

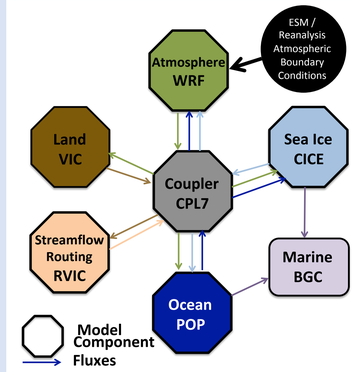

Figure 1. Wiring diagram for RASM showing model components and how fluxes are communicated among them.

Component	Code	Configuration
Atmosphere	WRF3	50km, 40 levels
Land	VIC	50km, 3 soil layers
Ocean	POP2	1/12º (~9km), 45 levels
Sea Ice	CICE6	1/12º (~9km), 5 thickness categories
Coupler	CPL7x	Flux exchange every 20 min

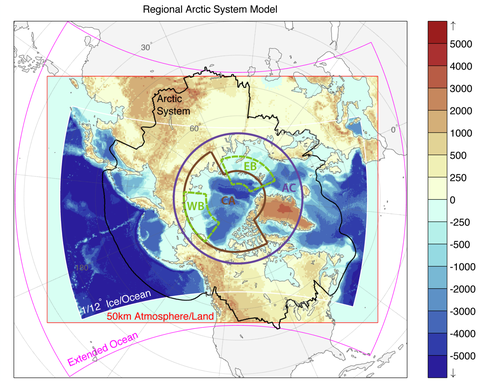

Figure 2. Model component domains, regions, and topography/bathymetry. The regions include: north of the Arctic Circle (66.56ºN; AC; purple line), the Central Arctic (CA; brown line), and the Western Bloom and Eastern Bloom (WB and EB, respectively, green dashed lines). The WB and EB regions were chosen to correspond to the analysis presented in Frants et al. (in prep), which showed that these locations consistently represented areas of high PP.

<- Table 1. Components, code and configuration of RASM. Please note that many configurations are available for RASM; this is the configuration for results shown here.

	Diatom chl-a				PP			
Ice concentration	CA	WB	EB	AC	CA	WB	EB	AC
≥50%	68.1	49.1	56.8	44.5	63.0	46.7	46.7	35.3
≥75%	58.5	38.3	44.4	35.7	52.3	35.9	33.8	26.5
≥85%	47.2	29.6	33.4	27.6	40.8	27.4	23.7	19.5
≥90%	31.7	17.1	21.7	18.2	25.7	15.4	13.9	11.9
≥99%	5.3	2.0	1.9	2.8	0.2	0.1	0.05	0.1

<- Table 2. Percentage of ice-covered pelagic diatom chl-*a* and PP in the upper 122m under various sea ice concentration thresholds. Percentages are averages over the simulation time period (1980-2018). Regional abbreviations are defined in Fig. 2.

Quantity	CA	WB	EB	AC
Diatom chl-a	2.91 (1.72, 4.11)	0.836 (0.0732, 1.60)	-0.496 (-1.19, 0.199)	1.86 (0.0195, 3.71)
PP	27.6 (19.7, 35.5)	8.98 (3.59, 14.38)	1.93 (-2.25, 6.12)	33.7 (20.9, 46.5)
Sea ice area	-0.0981 (-0.135, -0.0609)	-0.0434 (-0.0640, -0.0228)	-0.0287 (-0.0510, -0.00644)	-0.183 (-0.241, -0.125)
Sea ice volume	-0.129 (-1.50, -1.07)	-0.0127 (-0.0184, -0.00705)	-0.0195 (-0.0274, -0.0116)	-0.148 (-0.172, -0.123)

Table 3. Linear decadal trends (and 95% confidence bounds in parenthesis) in total diatom chl-*a* (Gg/decade), total PP (Gg C/decade), sea ice area (million km^2/decade), and sea ice volume (thousand km^3/decade) over the period simulation period (1980-2018) for various regions. Regional abbreviations are defined in Fig. 2.

METHODS

Coupled model simulations were run for the time period 1980-2018 after an initial 76-year spin-up integration for the physical (ocean and sea ice) components and an additional 9-year spin-up for the BGC components. Sea ice concentration is a model variable that quantifies the percentage of sea ice covering each model grid cell. A concentration of 50% means that half of the grid cell is sea ice-covered and half is sea ice-free.

In order to quantify the PP beneath sea ice with a concentration of ≥ 50%, we (1) integrated the PP over a depth of 0-122 m for each grid cell, (2) classified each model grid cell as either sea ice-covered or sea ice-free based on the concentration of sea ice present in each model grid cell, (3) summed the PP in sea ice-covered grid cells only across four regions [Central Arctic (CA), Western Bloom (WB), Eastern Bloom (EB), and Arctic Circle (AC)].

CONCLUSIONS

- Populations of **pelagic phytoplankton found beneath sea ice make up the bulk of PP in the central Arctic** and need to be observed throughout the region, particularly during the spring and early summer, to improve understanding of their contribution to the global carbon cycle.
- Although the model compares well with limited measurements of an ice-covered bloom (Frants et al. 2020), **more ice-covered observational data is needed** to confirm the commonality of annual springtime blooms in the western bloom region as shown by the model.
- The total PP in the CA region is **increasing at a rate of 5.2% per decade** during the period 1980-2018.
- We believe that more realistic model representation of ocean mesoscale dynamics (e.g. eddies), which requires further **increases in spatial resolution of the physical and biological model components**, should help improve simulation of the **large peaks and patchiness of biological variables** that occur in reality.

REFERENCES

Arrigo, K. R., & Van Dijken, G. L. (2011). Secular trends in Arctic Ocean net primary production. *Journal of Geophysical Research: Oceans*, *116*(9), 1–15.

Arrigo, K. R., Perovich, D. K., Pickart, R. S., Brown, Z. W., Dijken, G. L. Van,... Swift, J. H. (2012). Massive phytoplankton blooms under Arctic sea ice. *Science*, *336*, 1408.

Arrigo, K. R., Perovich, D. K., Pickart, R. S., Brown, Z. W., van Dijken, G. L., Lowry,... Swift, J. H. (2014). Phytoplankton blooms beneath the sea ice in the Chukchi sea. *Deep-Sea Research Part II: Topical Studies in Oceanography*, *105*, 1–16.

Cassano, J. J., DuVivier, A., Roberts, A., Hughes, M., Seefeldt, M., Brunke, M., Craig, A., Fisel, B., Gutowski, W., Hamman, J., Higgins, M., Maslowski, W., Nijssen, B., Osinski, R., & Zeng, X. (2017). Development of the Regional Arctic System Model (RASM): Near-surface atmospheric climate sensitivity. *Journal of Climate*, *30*(15), 5729–5753. https://doi.org/10.1175/JCLI-D-15-0775.1

DuVivier, A. K., Cassano, J. J., Craig, A., Hamman, J., Maslowski, W., Nijssen, B., Osinski, R., & Roberts, A. (2016). Winter atmospheric buoyancy forcing and oceanic response during strong wind events around southeastern Greenland in the Regional Arctic System Model (RASM) for 1990-2010. *Journal of Climate*, *29*(3), 975–994. https://doi.org/10.1175/JCLI-D-15-0592.1

Fukuchi, M., Watanabe, K., Tanimura, A., Hoshiai, T., Sasaki, H., Satoh, H., & Yamaguchi, Y. (1989). A phytoplankton bloom under sea ice recorded with a moored system in Lagoon Saroma Ko, Hokkaido, Japan. *Proc. Natl. Inst. Polar Res. (NIPR) Symp. Polar Biol.*, *2*, 9-15.

Hamman, J., Nijssen, B., Brunke, M., Cassano, J., Craig, A., DuVivier, A., Hughes, M., Lettenmaier, D. P., Maslowski, W., Osinski, R., Roberts, A., & Zeng, X. (2016). Land surface climate in the regional Arctic system model. *Journal of Climate*, *29*(18), 6543–6562.

Hamman, J., Nijssen, B., Roberts, A., Craig, A., Maslowski, W., & Osinski, R. (2017). The coastal streamflow flux in the Regional Arctic System Model. *Journal of Geophysical Research: Oceans*, *122*, 1683–1701.

Jin, M., Deal, C., Maslowski, W., Matrai, P., Roberts, A., Osinski, R., Lee, Y. J., Frants, M., Elliott, S., Jeffery, N., Hunke, E., & Wang, S. (2018). Effects of Model Resolution and Ocean Mixing on Forced Ice-Ocean Physical and Biogeochemical Simulations Using Global and Regional System Models. *Journal of Geophysical Research: Oceans*, *123*(1), 358–377. https://doi.org/10.1002/2017JC013365

Legendre, L., Ingram, R. G. Poulin, M. (1989). Physical control of phytoplankton production under sea ice (Manitounuk Sound, Hudson Bay). *Can. J. Fish. Aquat. Sci*, *38*, 1385–1392.

Lowry, K. E., van Dijken, G. L., & Arrigo, K. R. (2014). Evidence of under-ice phytoplankton blooms in the Chukchi Sea from 1998 to 2012. *Deep-Sea Research Part II: Topical Studies in Oceanography*, *105*, 105–117.

Maslowski, W., Clement Kinney, J., Higgins, M., & Roberts, A. (2012). The Future of Arctic Sea Ice. *Annual Review of Earth and Planetary Sciences*, *40*(1), 625–654. https://doi.org/10.1146/annurev-earth-042711-105345

Roberts, A., Craig, A., Maslowski, W., Osinski, R., Duvivier, A., Hughes, M., Nijssen, B., Cassano, J., & Brunke, M. (2015). Simulating transient ice-ocean Ekman transport in the Regional Arctic System Model and Community Earth System Model. *Annals of Glaciology*, *56*(69), 211–228. https://doi.org/10.3189/2015AoG69A760